Research Article Vol. 3, No. 10 / 15 October 2020 / OSA Continuum 2749

Scalar analytical expressions for the field dependence of Zernike polynomials in asymmetric optical systems with circular symmetric surfaces

ALESSANDRO GROSSO[1,2,*] AND TORALF SCHARF[2]

[1]Datalogic IP Tech Srl, Bologna, Italy
[2]Nanophotonics and Metrology Laboratory, EPFL, Lausanne, Switzerland
[*]alessandro.grosso@epfl.ch

Abstract: In this paper we derive scalar analytical expressions describing the full field dependence of Zernike polynomials in optical systems without symmetries. We consider the general case of optical systems constituted by arbitrarily tilted and decentered circular symmetric surfaces. The resulting analytical formulae are inferred from a modified version of the full field dependent wavefront aberration function proposed in the Nodal Aberration Theory (NAT). Such formula is modified with the scope of solving few critical points arising when primary and higher order aberrations are both present in an optical system. It is shown that when secondary aberrations are taken into account in the wavefront aberration function, the final effect is a perturbation to the symmetry of the field dependence of the Zernike polynomials. In particular, the centers of symmetry of the Zernike polynomial field dependences are shifted with respect to the locations predicted using the NAT equations as a consequence of the presence of higher order aberrations. The retrieved analytical expressions are verified through surface fitting to real ray-trace data obtained for a simple optical system.

1. Introduction

The Nodal Aberration Theory (NAT) proposed by Thompson [1,2] constitutes a fundamental step forward to the development of the wave theory of aberrations for non-circular symmetric optical systems characterized by tilted and decentered circular symmetric surfaces. NAT is built on the vectorial wavefront aberration formula introduced by Shack. Such vectorial expression is a reformulation of the scalar wavefront aberration formula introduced by H. H. Hopkins [3] for circular symmetric optical systems. NAT demonstrates that, in an optical system, the effect of geometrical perturbations such as tilt and decentering of optical surfaces, is to induce a particular nodal behavior in the field dependence of individual aberration types. This means that NAT provides a complete description of the aberration function of asymmetric optical systems as a function of both pupil and field coordinates.

An alternative description of the wavefront aberration function of an optical system is based on the use of Zernike polynomials. They represent a weighted polynomial expansion used to approximate the wavefront aberration function of any optical system with circular pupil. The weights of individual Zernike polynomial terms in the wavefront decomposition are represented by multiplicative coefficients retrieved with a polynomial fitting routine applied to the wavefront function itself. The Zernike polynomials decomposition is normally applied to pupil dependent wavefront functions whose field dependence is omitted because the wavefront function itself is referred to a single field point in the field of view (FOV) plane. Nevertheless, such polynomial expansion can be extended to a full field dependent wavefront aberration function, provided that the coefficients of the Zernike terms are turned into field dependent functions. This approach opens up the possibility of decomposing the four dimensional full field wavefront aberration

#396288 https://doi.org/10.1364/OSAC.396288
Journal © 2020 Received 27 Apr 2020; accepted 13 Sep 2020; published 27 Sep 2020

OSA CONTINUUM

function of an optical system in terms of analytical expressions consisting of the product between Zernike polynomials (depending on the pupil coordinates) and functions depending on the field coordinates.

In the design of optical systems where the full field behavior of aberrations is of concern, it is desirable to dispose of such analytical expressions. For example, the design of a multi-aperture optical system whose optical branches consist of decentered optical components can benefit of these formulae. Therefore, the main goal of the present work is to derive the full field dependence of Zernike polynomials for asymmetric optical systems constituted by tilted and decentered circular symmetric surfaces. For this purpose, it will be used a slightly modified version of the full field wavefront aberration function described in the NAT theory. In this regard, we will revisit partly the work done in [4]. Additionally, we aim at verifying numerically the expressions introduced in NAT to retrieve the location of the centers of symmetry in the FOV of primary aberrations in asymmetric optical systems. Finally, we validate the analytical expressions of the field dependence of Zernike polynomials with ray-trace based calculation obtained for a simple optical system constituted by a sequence of two tilted and decentered spherical lenses.

2. Full field wavefront aberration function in asymmetric optical systems with tilted and decentered circular symmetric surfaces

As said above, the Nodal Aberration theory was introduced to explain the occurrence of nodes in the full-field aberration function of optical systems characterized by tilted and decentered circular symmetric surfaces. The effect of surface tilt and decentering with respect to the mechanical axis of the system is modeled as a perturbation to the full field dependence of the aberration function of the optical system itself. The vectorial wavefront aberration function introduced by NAT is shown in Eq. (1) [1]

$$W(\vec{H},\vec{\rho}) = \sum_{j}\sum_{p}^{\infty}\sum_{n}^{\infty}\sum_{m}^{\infty}(W_{klm})_j((\vec{H}-\vec{\sigma}_j)\cdot(\vec{H}-\vec{\sigma}_j))^p(\vec{\rho}\cdot\vec{\rho})^n((\vec{H}-\vec{\sigma}_j)\cdot\vec{\rho})^m \tag{1}$$

where $\vec{\rho}$ is the pupil vector and $\vec{H}$ is the field vector. It can be defined an effective field vector $\vec{H}_{eff} = \vec{H} - \vec{\sigma}_j$ accounting for the perturbation induced by $\vec{\sigma}_j$, a vector in the FOV plane pointing to the center of symmetry of the aberration fields for individual tilted and decentered surfaces indexed with j. $(W_{klm})_j$ are the aberration coefficients of the surface j, identified by the indexes m, $k = 2p + m$ and $l = 2n + m$. Formally, Eq. (1) is the extension to asymmetric optical systems with circular symmetric surfaces of the formula introduced by Hopkins [3] to describe the aberrations in circular symmetric optical systems.

In [4], Eq. (1) is expanded up to secondary aberrations retaining the summation over the surfaces indexed with j. This formulation is valid in the case only primary aberrations are of concern, but it is no longer valid to describe the behavior of higher order aberrations for asymmetric optical systems consisting of circular symmetric surfaces. In this regard, we believe it is important to mention the following considerations. Relatively to circular symmetric optical systems, it is known that the contributions of primary aberrations can be added on a surface by surface base according to the summation theorem for primary aberration [5]. This theorem entails that, when higher order aberrations are taken into account, it is no longer possible to assume the validity of this summation. More precisely, the summation of aberration contributions from individual surfaces is valid under the assumption that the total wavefront aberration function of an optical system is not affected by a change of the radius of curvature of the reference sphere. This assumption is valid only for primary aberrations (being of 4^{th} order) since the change of the radius of the reference sphere determines a modification to the 6^{th} order of the wavefront error, thus having an impact on aberrations of order higher than the fourth [5,6]. Additionally, we mention that for higher order aberrations it is useful to discriminate between

OSA CONTINUUM

intrinsic and extrinsic aberrations where the former relates to a contribution that can be effectively ascribed to a surface j, while the latter relates to the contributions generated by the surfaces $1, \ldots, j-1$ preceding the surface j. Sasiàn addressed this problem retrieving a series of complex formulae to calculate secondary aberration coefficients in circular symmetric optical systems [7]. These observations lead us to consider in this paper a modified version of Eq. (1) relatively to asymmetric optical systems. Therefore, in order to avoid the aforementioned points of criticism, we remove from Eq. (1) the summation Σ_j over the surfaces of the optical system. Nevertheless, for the main purpose of this paper, that is the calculation of the field dependence of Zernike polynomials, we will retain the general structure of Eq. (1) which points out the possibility to identify different centers of symmetry in the field dependence of different aberration terms. Consequently, modifying Eq. (1) consistently with the previous considerations, we obtain the following Eq. (2) that is the starting point of our further derivation of the field dependence of Zernike polynomials

$$W(\vec{H},\vec{\rho}) = \sum_{p}^{\infty}\sum_{n}^{\infty}\sum_{m}^{\infty} W_{klm}((\vec{H}-\vec{a}_{klm})\cdot(\vec{H}-\vec{a}_{klm}))^{p}(\vec{\rho}\cdot\vec{\rho})^{n}((\vec{H}-\vec{a}_{klm})\cdot\vec{\rho})^{m}. \tag{2}$$

The coefficients W_{klm} and the displacement vectors $\vec{a}_{klm}$ denote respectively the net aberration coefficients and the net field displacement vectors of the total wavefront error of an asymmetric optical system. Equation (2) can be reduced to Eq. (1) under the condition that secondary and higher order aberrations are negligible with respect to primary aberrations, i.e. in optical systems with small apertures and small field angles. In this case, we can use the following Eq. (3) to calculate the net primary aberration coefficients and displacement vectors as shown in [1,2,8,9,10]:

$$\begin{cases} W_{klm} = \sum_{j} W_{klm,j} \\ \vec{a}_{klm} = \frac{\sum_{j} W_{klm,j}\vec{\sigma}_{j}}{W_{klm}} \end{cases}. \tag{3}$$

In Eq. (3), the summation over the surfaces j is valid supposing that the optical system is characterized predominantly by primary aberrations, in fact the coefficients W_{klm} are nothing but the Seidel sums [5]. On the other side, if we are concerned with higher order aberrations, the calculation of the coefficients W_{klm} and displacement vectors $\vec{a}_{klm}$ is no longer accurate if Eq. (3) are used. In this case, the displacement vectors $\vec{a}_{klm}$ related to primary aberrations are affected by the contribution of higher order aberrations and in addition to this, the coefficients W_{klm} cannot be simply calculated summing the aberration contributions of different surfaces in the optical system.

As mentioned above, in Eq. (2) we retain the general structure of Eq. (1) which highlights the possibility to identify a center of symmetry (located by the field displacement vector) in the field dependence of different aberration terms. Developing Eq. (2) up to the 6^{th} order, we obtain the following Eq. (4) describing the wavefront aberration function constituted by primary and secondary aberrations for asymmetric optical systems with tilted and decentered circular

OSA CONTINUUM

symmetric surfaces:

$$
\begin{aligned}
W(\vec{H},\vec{\rho}) &= W_{000} + W_{020}(\vec{\rho}\cdot\vec{\rho}) + W_{111}[(\vec{H}-\vec{a}_{111})\cdot\vec{\rho}] \\
&+ W_{040}(\vec{\rho}\cdot\vec{\rho})^2 + W_{131}[(\vec{H}-\vec{a}_{131})\cdot\vec{\rho}](\vec{\rho}\cdot\vec{\rho}) + W_{220}[(\vec{H}-\vec{a}_{220})\cdot(\vec{H}-\vec{a}_{220})](\vec{\rho}\cdot\vec{\rho}) \\
&+ W_{222}[(\vec{H}-\vec{a}_{222})\cdot\vec{\rho}]^2 + W_{311}[(\vec{H}-\vec{a}_{311})\cdot(\vec{H}-\vec{a}_{311})][(\vec{H}-\vec{a}_{311})\cdot\vec{\rho}] \\
&+ W_{060}(\vec{\rho}\cdot\vec{\rho})^3 + W_{151}[(\vec{H}-\vec{a}_{151})\cdot\vec{\rho}](\vec{\rho}\cdot\vec{\rho})^2 + W_{240}[(\vec{H}-\vec{a}_{240})\cdot(\vec{H}-\vec{a}_{240})](\vec{\rho}\cdot\vec{\rho})^2 \\
&+ W_{242}[(\vec{H}-\vec{a}_{242})\cdot\vec{\rho}]^2(\vec{\rho}\cdot\vec{\rho}) + W_{331}[(\vec{H}-\vec{a}_{331})\cdot(\vec{H}-\vec{a}_{331})][(\vec{H}-\vec{a}_{331})\cdot\vec{\rho}](\vec{\rho}\cdot\vec{\rho}) \\
&+ W_{333}[(\vec{H}-\vec{a}_{333})\cdot\vec{\rho}]^3 + W_{420}[(\vec{H}-\vec{a}_{420})\cdot(\vec{H}-\vec{a}_{420})][(\vec{H}-\vec{a}_{420})\cdot(\vec{H}-\vec{a}_{420})](\vec{\rho}\cdot\vec{\rho}) \\
&+ W_{422}[(\vec{H}-\vec{a}_{422})\cdot(\vec{H}-\vec{a}_{422})][(\vec{H}-\vec{a}_{422})\cdot\vec{\rho}]^2 \\
&+ W_{511}[(\vec{H}-\vec{a}_{511})\cdot(\vec{H}-\vec{a}_{511})][(\vec{H}-\vec{a}_{511})\cdot(\vec{H}-\vec{a}_{511})][(\vec{H}-\vec{a}_{511})\cdot\vec{\rho}]
\end{aligned}
\quad . \qquad (4)
$$

In general, the aberration coefficients W_{klm} in Eq. (4) are different from the aberration coefficients related to the wavefront aberration function of a corresponding circular symmetric optical system. As a matter of fact, expanding Eq. (4), it is obtained a power series in the ray coordinates containing terms of even and odd degree up to the 6^{th} order while the wavefront aberration function of a circular symmetric system contains only terms of even order. It is worth noting that if secondary aberrations give a significant contribution to the total wavefront aberration function in Eq. (4), then several lower order terms (of both even and odd order) are generated and added to the terms attributable to primary aberrations. Therefore, in Eq. (4) the displacement vectors locating the centers of symmetry of the field dependence of primary aberrations are influenced by the presence of higher order aberrations. Such perturbative effect of higher order aberrations on primary aberrations is treated in [9,10] where effective aberration coefficients and effective field displacement vectors are introduced to account for the shift induced by secondary aberrations.

In Eq. (4) each aberration term exhibits a center of symmetry that in general does not coincide with a node location for the specific aberration type. In particular, as regards binodal astigmatism, the vector $\vec{a}_{222}$ locates the intermediate position in the FOV plane between the two nodes characterizing this aberration type. Equivalently, the vector $\vec{a}_{222}$ indicates the center of symmetry of primary astigmatism in the FOV plane in a non-circular symmetric optical system. On the other hand, regarding primary coma the vector $\vec{a}_{131}$ locates at the same time the center of symmetry of this aberration and the position of its single node in the FOV plane.

In order to retrieve the field dependence of Zernike coefficients in asymmetric optical systems, we proceed to convert Eq. (4) into a scalar form. The reference system used in this work is shown in Fig. 1.

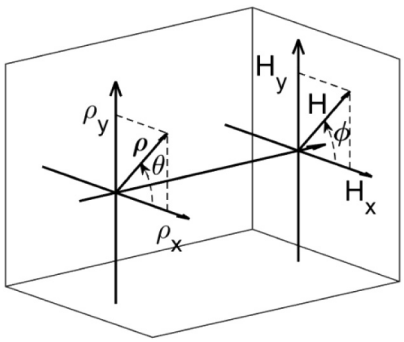

Fig. 1. Reference system.

OSA CONTINUUM

The vectors $\vec{\rho}$, $\vec{H}$ and $\vec{a}_{klm}$ are respectively

$$\vec{\rho} = \begin{pmatrix} \rho_x \\ \rho_y \end{pmatrix} = \begin{pmatrix} \rho\cos\vartheta \\ \rho\sin\vartheta \end{pmatrix}$$
$$\vec{H} = \begin{pmatrix} H_x \\ H_y \end{pmatrix} = \begin{pmatrix} H\cos\varphi \\ H\sin\varphi \end{pmatrix}. \tag{5}$$
$$\vec{a}_{klm} = \begin{pmatrix} a_{klm,x} \\ a_{klm,y} \end{pmatrix}$$

Using the expression exposed by Thompson in [1,2] to calculate the square of a generic vector $\vec{v} = v_x\vec{i} + v_y\vec{j}$ (where $\vec{v} = ve^{i\alpha} = v\cos\alpha\vec{i} + v\sin\alpha\vec{j}$)

$$(\vec{v})^2 = \begin{pmatrix} v_x \\ v_y \end{pmatrix}^2 = \begin{pmatrix} v\cos 2\alpha \\ v\sin 2\alpha \end{pmatrix} = \begin{pmatrix} v_x^2 - v_y^2 \\ 2v_xv_y \end{pmatrix} \tag{6}$$

one obtains the following series of equations from Eq. (7) to Eq. (15) for all primary aberrations and only few secondary aberrations. Among them, we consider oblique spherical aberration W_{OSA}, field cubed coma W_{CC}, secondary field curvature W_{FC2} and secondary astigmatism W_{A2}. These secondary aberrations are explicitly considered because they give a more consistent contribution to the field dependence of Zernike coefficients shown below in the ray-trace based example. The complete scalar full field wavefront aberration function $W(H_x, H_y, \rho, \vartheta)$ for asymmetric optical systems constituted by tilted and decentered circular symmetric surfaces is finally given by the sum of terms exposed in equations from Eq. (7) to Eq. (15).

We obtain for primary spherical aberration $W_{SA}(H_x, H_y, \rho, \vartheta)$ the well-known field independent expression in Eq. (7):

$$W_{SA}(H_x, H_y, \rho, \vartheta) = W_{040}\left[\begin{pmatrix} \rho\cos\vartheta \\ \rho\sin\vartheta \end{pmatrix}^T \cdot \begin{pmatrix} \rho\cos\vartheta \\ \rho\sin\vartheta \end{pmatrix}\right]^2 = .$$
$$W_{040}(\rho^2\cos^2\vartheta + \rho^2\sin^2\vartheta)^2 = W_{040}\rho^4 \tag{7}$$

For primary coma $W_C(H_x, H_y, \rho, \vartheta)$, one obtains Eq. (8):

$$W_C(H_x, H_y, \rho, \vartheta) = W_{131}\left[\begin{pmatrix} H_x - a_{131,x} \\ H_y - a_{131,y} \end{pmatrix}^T \cdot \begin{pmatrix} \rho\cos\vartheta \\ \rho\sin\vartheta \end{pmatrix}\right]\left[\begin{pmatrix} \rho\cos\vartheta \\ \rho\sin\vartheta \end{pmatrix}^T \cdot \begin{pmatrix} \rho\cos\vartheta \\ \rho\sin\vartheta \end{pmatrix}\right] = .$$
$$W_{131}[(H_x - a_{131,x})\rho\cos\vartheta + (H_y - a_{131,y})\rho\sin\vartheta](\rho^2\cos^2\vartheta + \rho^2\sin^2\vartheta) =$$
$$W_{131}[(H_x - a_{131,x})\rho^3\cos\vartheta + (H_y - a_{131,y})\rho^3\sin\vartheta] \tag{8}$$

For primary astigmatism $W_A(H_x, H_y, \rho, \vartheta)$., one obtains Eq. (9):

$$W_A(H_x, H_y, \rho, \vartheta) = \frac{1}{2}W_{222}\left[\begin{pmatrix} H_x - a_{222,x} \\ H_y - a_{222,y} \end{pmatrix}^2\right]^T \cdot \begin{pmatrix} \rho\cos\vartheta \\ \rho\sin\vartheta \end{pmatrix}^2 = .$$
$$\frac{1}{2}W_{222}\begin{bmatrix} ((H_x - a_{222,x})^2 - (H_y - a_{222,y})^2)\rho^2\cos 2\vartheta \\ +2(H_x - a_{222,x})(H_y - a_{222,y})\rho^2\sin 2\vartheta \end{bmatrix} \tag{9}$$

OSA CONTINUUM

Relatively to field curvature $W_{FC}(H_x, H_y, \rho, \vartheta)$, one obtains the following Eq. (10):

$$W_{FC}(H_x, H_y, \rho, \vartheta) = \\ W_{220}\left[\begin{pmatrix} H_x - a_{220,x} \\ H_y - a_{220,y} \end{pmatrix}^T \cdot \begin{pmatrix} H_x - a_{220,x} \\ H_y - a_{220,y} \end{pmatrix}\right]\left[\begin{pmatrix} \rho\cos\vartheta \\ \rho\sin\vartheta \end{pmatrix}^T \cdot \begin{pmatrix} \rho\cos\vartheta \\ \rho\sin\vartheta \end{pmatrix}\right] =. \\ W_{220}[(H_x - a_{220,x})^2 + (H_y - a_{220,y})^2]\rho^2 \tag{10}$$

For Eq. (9) and Eq. (10) we have considered that field curvature and primary astigmatism are referred to the medial astigmatic surface setting $W_{220} = W_{220S} + \frac{W_{222}}{2}$ (where the subscript of the term W_{220S} stands for *Sagittal*). For distortion $W_D(H_x, H_y, \rho, \vartheta)$, we obtain Eq. (11):

$$W_D(H_x, H_y, \rho, \vartheta) = \\ W_{311}\left[\begin{pmatrix} H_x - a_{311,x} \\ H_y - a_{311,y} \end{pmatrix}^T \cdot \begin{pmatrix} H_x - a_{311,x} \\ H_y - a_{311,y} \end{pmatrix}\right]\left[\begin{pmatrix} H_x - a_{311,x} \\ H_y - a_{311,y} \end{pmatrix}^T \cdot \begin{pmatrix} \rho\cos\vartheta \\ \rho\sin\vartheta \end{pmatrix}\right] = \quad . \\ W_{311}[(H_x - a_{311,x})^2 + (H_y - a_{311,y})^2][(H_x - a_{311,x})\rho\cos\vartheta + (H_y - a_{311,y})\rho\sin\vartheta] \tag{11}$$

For oblique spherical aberration $W_{OSA}(H_x, H_y, \rho, \vartheta)$, we obtain Eq. (12) similar to Eq. (10) for field curvature regarding the only field dependence:

$$W_{OSA}(H_x, H_y, \rho, \vartheta) = W_{240}\left[\begin{pmatrix} H_x - a_{240,x} \\ H_y - a_{240,y} \end{pmatrix}^T \cdot \begin{pmatrix} H_x - a_{240,x} \\ H_y - a_{240,y} \end{pmatrix}\right]\left[\begin{pmatrix} \rho\cos\vartheta \\ \rho\sin\vartheta \end{pmatrix}^T \cdot \begin{pmatrix} \rho\cos\vartheta \\ \rho\sin\vartheta \end{pmatrix}\right]^2 = \\ W_{240}[(H_x - a_{240,x})^2 + (H_y - a_{240,y})^2]\rho^4 \tag{12}$$

In Eq. (12) the coefficient W_{240} is defined as $W_{240} = W_{240S} + \frac{W_{242}}{2}$ in order to reference it to the medial surface. For field cubed coma $W_{CC}(H_x, H_y, \rho, \vartheta)$, we obtain Eq. (13) similar to Eq. (11) obtained for distortion (concerning the only field behavior):

$$W_{CC}(H_x, H_y, \rho, \vartheta) = \\ W_{331M}\left[\begin{pmatrix} H_x - a_{331,x} \\ H_y - a_{331,y} \end{pmatrix}^T \cdot \begin{pmatrix} H_x - a_{331,x} \\ H_y - a_{331,y} \end{pmatrix}\right] \\ \left[\begin{pmatrix} H_x - a_{331,x} \\ H_y - a_{331,y} \end{pmatrix}^T \cdot \begin{pmatrix} \rho\cos\vartheta \\ \rho\sin\vartheta \end{pmatrix}\right]\left[\begin{pmatrix} \rho\cos\vartheta \\ \rho\sin\vartheta \end{pmatrix}^T \cdot \begin{pmatrix} \rho\cos\vartheta \\ \rho\sin\vartheta \end{pmatrix}\right] = \quad . \\ W_{331M}[(H_x - a_{331,x})^2 + (H_y - a_{331,y})^2] \\ [(H_x - a_{331,x})\rho\cos\vartheta + (H_y - a_{331,y})\rho\sin\vartheta](\rho^2\cos^2\vartheta + \rho^2\sin^2\vartheta) = \\ W_{331}[(H_x - a_{331,x})^2 + (H_y - a_{331,y})^2][(H_x - a_{331,x})\rho^3\cos\vartheta + (H_y - a_{331,y})\rho^3\sin\vartheta] \tag{13}$$

In Eq. (13) the coefficient W_{331M} is defined as $W_{331M} = W_{331} + \frac{3}{4}W_{333}$. This implies that it contains part of trefoil aberration weighted by the coefficient W_{333}. For secondary field curvature

OSA CONTINUUM

$W_{FC2}(H_x, H_y, \rho, \vartheta)$, we obtain Eq. (14):

$$W_{FC2}(H_x, H_y, \rho, \vartheta) = W_{420}\left[\begin{pmatrix} H_x - a_{420,x} \\ H_y - a_{420,y} \end{pmatrix}^T \cdot \begin{pmatrix} H_x - a_{420,x} \\ H_y - a_{420,y} \end{pmatrix}\right]$$
$$\left[\begin{pmatrix} H_x - a_{420,x} \\ H_y - a_{420,y} \end{pmatrix}^T \cdot \begin{pmatrix} H_x - a_{420,x} \\ H_y - a_{420,y} \end{pmatrix}\right]\left[\begin{pmatrix} \rho\cos\vartheta \\ \rho\sin\vartheta \end{pmatrix}^T \cdot \begin{pmatrix} \rho\cos\vartheta \\ \rho\sin\vartheta \end{pmatrix}\right] = \tag{14}$$
$$W_{420}[(H_x - a_{420,x})^2 + (H_y - a_{420,y})^2]^2\rho^2$$

Finally, for secondary astigmatism $W_{A2}(H_x, H_y, \rho, \vartheta)$, we obtain Eq. (15):

$$W_{A2}(H_x, H_y, \rho, \vartheta) = \frac{1}{2}W_{422}\left[\begin{pmatrix} H_x - a_{422,x} \\ H_y - a_{422,y} \end{pmatrix}^T \cdot \begin{pmatrix} H_x - a_{422,x} \\ H_y - a_{422,y} \end{pmatrix}\right]$$
$$\left[\left(\begin{pmatrix} H_x - a_{422,x} \\ H_y - a_{422,y} \end{pmatrix}^2\right)^T \cdot \begin{pmatrix} \rho\cos\vartheta \\ \rho\sin\vartheta \end{pmatrix}^2\right] = \tag{15}$$
$$\frac{1}{2}W_{422}[(H_x - a_{422,x})^2 + (H_y - a_{422,y})^2]$$
$$[((H_x - a_{422,x})^2 - (H_y - a_{422,y})^2)\rho^2\cos 2\vartheta + 2(H_x - a_{422,x})(H_y - a_{422,y})\rho^2\sin 2\vartheta]$$

To be noted that in Eqs. (14) and (15), similarly with what we have done previously for primary field curvature and primary astigmatism, we have set $W_{420} = W_{420S} + \frac{W_{422}}{2}$ in order to fix the medial astigmatic surface as reference.

The total scalar full field dependent and pupil dependent wavefront aberration function $W(H_x, H_y, \rho, \vartheta)$ results from the sum of individual aberration terms reported from Eq. (7) to Eq. (15). The remaining secondary aberration terms are not mentioned in this work because they are less relevant in the ray-trace data used for verification in the last paragraph. The scalar wavefront aberration function $W(H_x, H_y, \rho, \vartheta)$ is used in the following part to retrieve the field behavior of Zernike coefficients in asymmetric optical systems constituted by tilted and decentered surfaces.

3. Full field dependence of Zernike polynomials in asymmetric systems

As said before, in this paper we partly revisit the work done in [4] using a slightly different version of the full field wavefront aberration function proposed in NAT. Such reformulation of the wavefront aberration function is essentially designed to avoid contradictions with the summation theorem for primary aberrations. In this section, we derive the full field dependence of Zernike polynomials for asymmetric optical systems with circular symmetric surfaces. In the last section, we provide a numerical verification of the expressions derived in the present section.

Zernike polynomials, indicated in this work as $C_n^m(\rho, \vartheta)$, are a complete set of polynomials depending on the radial and azimuthal coordinates of the pupil. They are orthonormal in a continuous fashion over the interior of a unit circle and are expressed as the product of a polynomial function $R_n^m(\rho)$ depending only on the radial coordinate and a trigonometric function $G^m(\vartheta)$ depending only on the azimuthal coordinate. In detail, they are described as follows:

$$C_n^m(\rho, \vartheta) = F_n^m R_n^m(\rho) G^m(\vartheta) = F_n^m Z_n^m(\rho, \vartheta) \tag{16}$$

where F_n^m are the Zernike coefficient and $Z_n^m(\rho, \vartheta)$ are pupil dependent functions resulting from the product between $R_n^m(\rho)$ and $G^m(\vartheta)$. We use the Fringe indexing scheme. Similarly to what

OSA CONTINUUM

has been shown by Gray et al. [11] for the case of circular symmetric optical systems, the computation of the field dependence of Zernike coefficients in asymmetric optical systems is retrieved projecting the scalar full field dependent and pupil dependent wavefront aberration function $W(H_x, H_y, \rho, \vartheta)$ into the Zernike polynomial basis. Equivalently, the field dependent coefficients of individual Zernike polynomials in asymmetric optical systems are obtained computing the following double integral with respect to the polar coordinates of the pupil shown in Eq. (17):

$$F_n^m(H_x, H_y) = \frac{1}{N_{nm}} \int_0^{2\pi} \int_0^1 W(H_x, H_y, \rho, \vartheta) Z_n^m(\rho, \vartheta) \rho d\rho d\vartheta \tag{17}$$

where N_{nm} is the norm of Zernike polynomials. The computation of Eq. (17) results in a new expression [Eq. (18)] for the full field wavefront aberration function in asymmetric optical systems described as the sum of full field dependent Zernike polynomials. Individual terms in Eq. (18) are given by the product between the field dependent coefficients $F_n^m(H_x, H_y)$ retrieved with Eq. (17) and the respective Zernike polynomials $Z_n^m(\rho, \vartheta)$. The field dependent terms $F_n^m(H_x, H_y)$ in Eq. (18) are determined by the contributions from various aberration types with different centers of symmetry and weighted by their respective wave aberration coefficients W_{klm}. The field dependent functions $F_n^m(H_x, H_y)$ are actually power series containing terms of even and odd order in the field coordinates originated by the absence of a well-defined symmetry in optical systems with displaced and tilted components:

$$\begin{aligned}
&W(H_x, H_y, \rho, \vartheta) = \\
&\left[\begin{array}{l} \frac{W_{020}}{2} + \frac{W_{040}}{3} + \frac{W_{220}}{2}((H_x - a_{220,x})^2 + (H_y - a_{220,y})^2) + \\ \frac{W_{420}}{2}((H_x - a_{420,x})^2 + (H_y - a_{420,y})^2)^2 \end{array}\right] Z_0^0(\rho, \vartheta) + \\
&\left[\begin{array}{l} W_{111}(H_x - a_{111,x}) + \frac{2W_{131}}{3}(H_x - a_{131,x}) + \\ \frac{2W_{331}}{3}((H_x - a_{331,x})^2 + \quad (H_y - a_{331,y})^2)(H_x - a_{331,x}) \end{array}\right] Z_1^1(\rho, \vartheta) + \\
&\left[\begin{array}{l} W_{111}(H_y - a_{111,y}) + \frac{2W_{131}}{3}(H_y - a_{131,y}) + \\ \frac{2W_{331}}{3}((H_x - a_{331,x})^2 + (H_y - a_{331,y})^2)(H_y - a_{331,y}) \end{array}\right] Z_1^{-1}(\rho, \vartheta) + \\
&\left[\begin{array}{l} \frac{W_{020}}{2} + \frac{W_{040}}{2} + \frac{W_{220}}{2}((H_x - a_{220,x})^2 + (H_y - a_{220,y})^2) + \\ \frac{W_{420}}{2}((H_x - a_{420,x})^2 + (H_y - a_{420,y})^2)^2 \end{array}\right] Z_2^0(\rho, \vartheta) + \\
&\left[\begin{array}{l} \frac{W_{222}}{2}((H_x - a_{222,x})^2 - (H_y - a_{222,y})^2) + \\ \frac{W_{422}}{2}((H_x - a_{422,x})^4 - (H_y - a_{422,y})^4) \end{array}\right] Z_2^2(\rho, \vartheta) + \\
&\left[\begin{array}{l} W_{222}(H_x - a_{222,x})(H_y - a_{222,y}) + \\ W_{422}(((H_x - a_{422,x})^2 + (H_y - a_{422,y})^2)(H_x - a_{422,x})(H_y - a_{422,y})) \end{array}\right] Z_2^{-2}(\rho, \vartheta) + \\
&\left[\begin{array}{l} \frac{W_{131}}{3}(H_x - a_{131,x}) + \\ \frac{W_{331}}{3}((H_x - a_{331,x})^2 + (H_y - a_{331,y})^2)(H_x - a_{331,x}) \end{array}\right] Z_3^1(\rho, \vartheta) + \\
&\left[\begin{array}{l} \frac{W_{131}}{3}(H_y - a_{131,y}) + \\ \frac{W_{331}}{3}((H_x - a_{331,x})^2 + (H_y - a_{331,y})^2)(H_y - a_{331,y}) \end{array}\right] Z_3^{-1}(\rho, \vartheta) + \\
&\left[\frac{W_{040}}{6} + \frac{W_{240}}{6}((H_x - a_{240,x})^2 + (H_y - a_{240,y})^2)\right] Z_4^0(\rho, \vartheta)
\end{aligned} \tag{18}$$

OSA CONTINUUM

The terms in Eq. (18) correspond to the first nine Zernike polynomials using the Fringe indexing scheme. These terms are at most of 4^{th} order in their pupil coordinates dependence. Considering instead their field coordinates dependence, Eq. (18) explicitly shows that in an asymmetric optical system the full field behavior of Zernike polynomials is described by a superposition of polynomial surfaces whose respective displacements in the FOV plane are defined by the centers of symmetry of the inherent aberration types contributing to the description of the Zernike terms in question. In fact, we see that considering explicitly the contributions from the only primary aberrations (setting to zero the wave coefficients W_{klm} related to secondary aberrations), the field dependence of Zernike polynomials in asymmetric optical systems is unchanged with respect to their field dependence in circular symmetric optical systems, the only difference being that in the former case the full field behavior of Zernike polynomials exhibits a new center of symmetry displaced from the origin of the FOV plane. On the other hand, taking into consideration the contributions to the full field dependence of Zernike terms deriving jointly from primary and secondary aberrations, we can observe that in an asymmetric optical system the field dependence of each Zernike term no longer exhibits a well-defined symmetry because of the concomitant contribution of different order terms, in fact it results from the superposition of field surfaces with not coincident centers of symmetry.

From the above derivation, the resulting Eq. (18) demonstrates that the co-presence of primary and secondary aberrations modifies the symmetry of the field behavior of individual Zernike polynomials. In addition to this, when higher order field surfaces (related to secondary aberrations) are overlaid to lower order field surfaces (related to primary aberrations), the centers of symmetry of the latter can be displaced in the FOV plane. In optical systems where only primary aberrations are considered to contribute to the wavefront deformation, the aberration coefficients W_{klm} and the centers of symmetry of the field dependence of Zernike polynomials $\vec{a}_{klm}$ can be calculated using Eq. (3). In this specific case, using Eq. (3) to calculate the total primary aberration coefficients W_{klm}, is equivalent to assume that tilts and displacements of the surfaces in the optical system under study induce weak perturbations to the original symmetry of the system. In the following section, we compare the analytical result obtained in this section with ray tracing data calculated for a simple optical system. Additionally, we calculate the centers of symmetry of primary aberrations using Eq. (3) (derived from NAT) in order to compare the prediction of NAT equations with real ray tracing data.

4. Validation of results

To validate the analytical expressions describing the full field behavior of Zernike coefficients in asymmetric optical systems shown in the previous section, we compare them with real ray tracing data obtained for a simple system constituted by the sequence of two tilted and decentered plano-convex spherical lenses. The 3D layout of the optical system under study is shown in Fig. 2.

The system is at infinite conjugates. The aperture stop position is at the first surface (plane surface) of the first spherical lens L1 and the entrance pupil diameter is $ENPD = 10mm$. The simulation wavelength is $\lambda = 0.55\mu m$ and the FOV is 40° x 40°. It is worth to point out that the field coordinates in the FOV plane can be equivalently described in terms of object height or image height. We represent the field coordinates H_x and H_y in terms of field angles in degrees measured with respect to the object space z axis and the paraxial entrance pupil position (in this example located in correspondence of the plane surface of L1 where it is also located the aperture stop of the optical system) [12]. The spherical lenses are tilted and decentered with respect to the mechanical axis of the system as reported in Table 1. The distance between the two lenses is 20 mm. The image plane is at 292.4mm from the last optical surface. This distance has been chosen to minimize the RMS wavefront error and to constrain the defocus aberration to be zero for the

OSA CONTINUUM

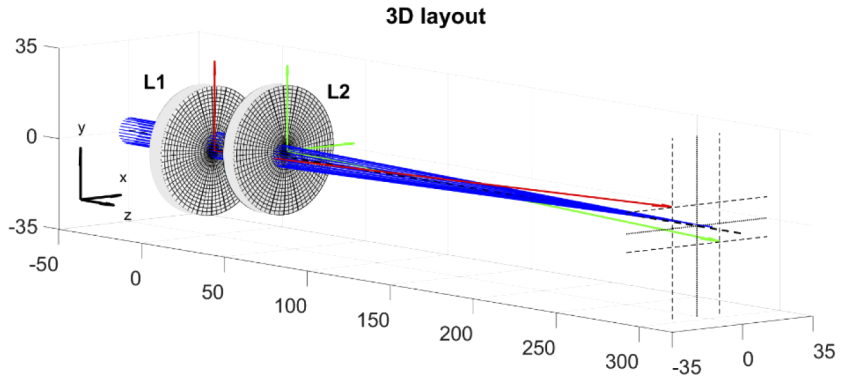

Fig. 2. 3D layout and reference system of the optical system under study (the dimensions are in mm). The lenses are indicated respectively with L1 and L2. In red and green are highlighted the local coordinate systems of the curved surfaces in both plano-convex spherical lenses.

field point ($H_x = 0°, H_y = 0°$). The parameters used for this example are summarized in Table 1. The simulation is performed in Zemax OpticStudio [12].

Table 1. Simulation parameters.

	Parameter	Symbol	Value
L1	Diameter	D_1	50 mm
	Radius of curvature	R_1	−400 mm
	Thickness	t_1	7 mm
	Glass	g_1	N-BK7
	Conic constant	c_1	0
	x decentering	$D_{x,1}$	−2 mm
	y decentering	$D_{y,1}$	−2 mm
	x tilt	$\tau_{x,1}$	−2 °
	y tilt	$\tau_{y,1}$	−2 °
L2	Diameter	D_2	50 mm
	Radius of curvature	R_2	−250 mm
	Thickness	t_2	5 mm
	Glass	g_2	N-BK7
	Conic constant	c_2	0
	x decentering	$D_{x,2}$	2 mm
	y decentering	$D_{y,2}$	2 mm
	x tilt	$\tau_{x,2}$	2 °
	y tilt	$\tau_{y,2}$	2 °

In Table 2 we report the values of the Seidel aberration coefficients in waves for the circular symmetric version of the optical system under test obtained setting to zero the parameters related to tilt and displacement of the two lenses L1 and L2.

The coefficients $W_{220,S}$ reported in Table 2 are the sagittal field curvature Seidel terms. The Seidel coefficients related to spherical aberration are not reported because this aberration is independent on the field angle, while those related to distortion are not reported because in

OSA CONTINUUM

Table 2. Seidel coefficients and displacement vectors.

	W_{131} (λ)	W_{222} (λ)	$W_{220,S}$ (λ)	σ_x (°)	σ_y (°)
L1	−0.2956	8.2344	6.9259	−1.55	2.44
L2	−0.9095	7.2874	8.1377	1.55	−3.25
TOT	−1.2051	15.5217	10636		

the following we neglect this aberration type (the reason of this will be clarified later). The calculation of the vectors $\vec{\sigma} = (\sigma_x, \sigma_y)$ is performed using the real ray tracing method exposed in [13]. In this example, the $\vec{\sigma}$ vectors are calculated for the lenses L1 and L2. In Fig. 3 are shown the $\vec{\sigma}$ vectors describing the field perturbations due to decentering (in blue) and tilt (in red) of the lenses L1 (in the upper part) and L2 (in the bottom part of the graph). The final displacement vectors (in green) result from the cumulative effect of decentering and tilt respectively for L1 and L2.

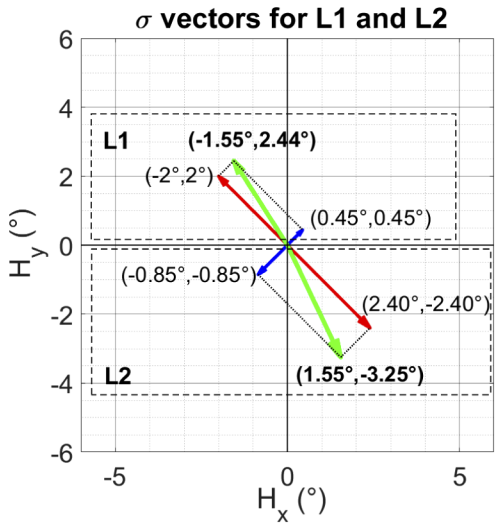

Fig. 3. Field displacement vectors in the FOV plane.

In what follows, we propose a quantitative comparison between numerical data simulated with ray tracing and the surface models shown in Eq. (18) corresponding to the field behavior of the first nine Zernike coefficients $F_n^m(H_x, H_y)$ in the Fringe indexing scheme. The verification of the proposed analytical expressions is carried out fitting the surface models $F_n^m(H_x, H_y)$ to the ray-trace data. The RMSE (Root Mean Squared Error) and SSE (Sum of Squares due to Error) of the fitting process are indicated to report on the goodness of the fit along with the values of the parameters in the equations of the model surfaces for the full field dependence of the Zernike coefficients. The ray-trace data shown in the following figures from Fig. 4 to Fig. 12 result from the computation of the respective Zernike coefficient over a grid of 101×101 field points. For each of these field points a grid of 128×128 rays is traced through the exit pupil of the optical system. The resulting wavefront matrix (with 128×128 elements) contains the optical path difference of the rays with respect to the reference sphere in correspondence of their intersection points with it. From the retrieved wavefront data, the mean value is subtracted and it is calculated the square root of its variance. Therefore, the data contained in the wavefront aberration matrix for each field point correspond to the RMS wavefront error referenced to its mean [6,12]. In the calculation of the optical path difference of light rays, the reference sphere is centered on the

OSA CONTINUUM

chief ray and its radius is equal to the distance between the exit pupil and the image plane of the optical system (in this example the exit pupil is located 322mm before the image plane).

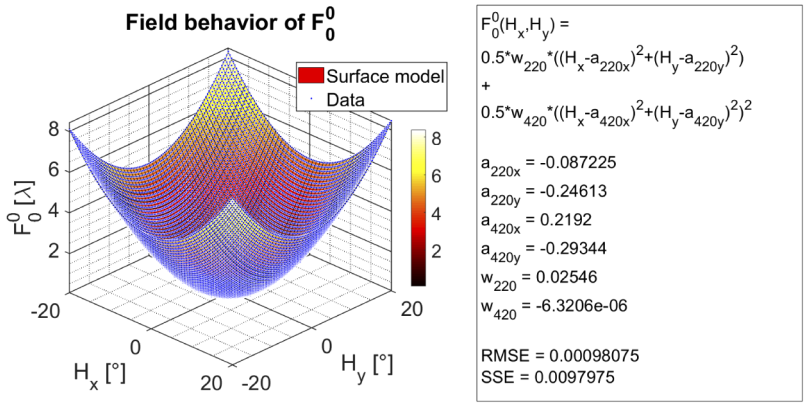

Fig. 4. Surface fitting of the field dependence of the first Zernike coefficient ($m = 0, n = 0$).

The surface models $F_n^m(H_x, H_y)$ used to fit the ray-trace data and indicated in the text box on the right side of every figure contain only the most relevant contributions from the constituting aberration types. More in detail, considering the example in Fig. 4 and recalling from Eq. (18) that the complete expression of $F_0^0(H_x, H_y)$ contains also the contributions of defocus (W_{020}) and primary spherical aberrations (W_{040}) in addition to those of primary field curvature (W_{220}) and secondary spherical aberration (W_{420}), in the surface fitting model $F_0^0(H_x, H_y)$ we have omitted the coefficients W_{020} and W_{040} because, as said before, the last surface to image distance of the optical system has been optimized to minimize the RMS wavefront error and the defocus term in correspondence of the center of the FOV (this implies that the coefficient W_{020} is always zero in the fitting models and the contribution of the coefficient W_{040} is encompassed in the contribution of other terms).

In Fig. 4 the full field behavior of the first Zernike coefficient is given by the superposition of a quadratic and a quartic surface respectively represented by primary field curvature and secondary spherical aberration. The contribution of oblique spherical aberration (W_{240}) is omitted in this case because such term exhibits the same quadratic dependence on the field coordinates as primary field curvature. These two overlapped polynomial surfaces exhibit different centers of symmetry. The contribution of primary field curvature to the field dependence of this Zernike polynomial is dominant for small FOV. When a wider FOV is required, the contribution from oblique spherical aberration becomes more and more relevant.

In Figs. 5 and 6 the surface fitting of the second and third Zernike coefficients full field behavior is carried out neglecting the contribution of distortion $W_D(H_x, H_y, \rho, \vartheta)$ because this aberration type does not degrade the image quality formed by an optical system. In fact, distortion is an image shape aberration measured differently from other aberrations. In particular, it is quantified tracing a grid of chief rays through the optical system and measuring the difference between the predicted and the real landing coordinates of such chief rays in the image plane. On the other side, the RMS wavefront error calculated for a specific field point is the optical path length difference of light rays over the pupil with respect to the chief ray. Therefore, the calculation of the RMS wavefront error does not account for distortion because the reference sphere is centered on the chief ray. From the fitting results in Fig. 5 and Fig. 6, we can observe that the centers of symmetry of the field dependence of the second and third Zernike coefficients, describing a displacement along the H_x (Fig. 5) and H_y (Fig. 6) directions, is located in the field point

OSA CONTINUUM

$\begin{pmatrix} a_{131,x} \\ a_{131,y} \end{pmatrix} = \begin{pmatrix} 0.92986° \\ -1.8202° \end{pmatrix}$ that represents the center of symmetry and also the node location of primary coma. This is also a consequence of the fact that the fitting models F_1^1 and F_1^{-1} do not include the linear displacement aberration W_{111} (boresight error) because its contribution is subtracted out from the calculation of the wavefront phase. This is justified because W_{111} shifts the image location but otherwise has no effect on image quality. Thus, the same result obtained for F_1^1 and F_1^{-1} will be obtained in the case of higher order Zernike terms F_3^1 and F_3^{-1} related to primary coma. Notice that the coefficients W_{131} and W_{331} almost coincide in Figs. 5 and 6. These values are retrieved later as concerns the field dependence of Zernike polynomials F_3^1 and F_3^{-1} because, as explained above, from the calculation of F_1^1 and F_1^{-1} has been removed the contribution given by the field displacement term locating the center of the shifted image plane. The coefficients W_{131} and W_{331} are the wavefront aberration coefficients weighting the magnitude of primary coma and field-cubed secondary coma. The calculation of the primary coma node location using Eq. (3) gives the following result $\begin{pmatrix} a_{131,x} \\ a_{131,y} \end{pmatrix} = \begin{pmatrix} 0.7877° \\ -1.8568° \end{pmatrix}$. The slight difference with the surface fitting result is probably due to the relevant contribution of higher order aberration terms such as field-cubed coma W_{331} that can shift the node position of a lower order aberration terms such as primary coma as discussed in [9].

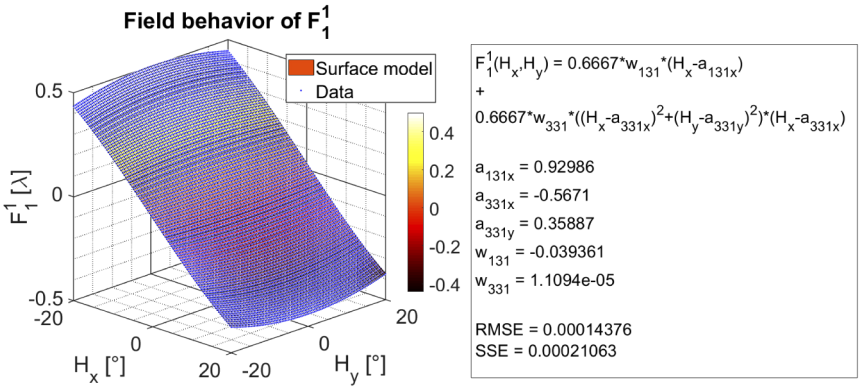

Fig. 5. Surface fitting of the field dependence of the second Zernike coefficient ($m = 1, n = 1$).

The surface fitting result in Fig. 7, related to the field dependence of the fourth Zernike Fringe coefficient, coincides with the result previously obtained for the first Zernike Fringe coefficient. This is due to the fact that both Zernike coefficients (the first and the fourth) exhibit the same dependence on the field coordinates but different behavior with respect to the pupil coordinates; in fact, the first one is a piston-like term while the fourth is a defocus term. The location of primary field curvature node, calculated using Eq. (3), is $\begin{pmatrix} a_{220,x} \\ a_{220,y} \end{pmatrix} = \begin{pmatrix} 0.0503° \\ -0.5021° \end{pmatrix}$. This calculation is referenced to the medial focal surface according to [1] using the data in Table 2. The mismatch with the ray tracing data $\begin{pmatrix} a_{220,x} \\ a_{220,y} \end{pmatrix} = \begin{pmatrix} -0.086096° \\ -0.24654° \end{pmatrix}$ is attributed to the significance of secondary aberration due to the wide FOV considered in this example.

OSA CONTINUUM

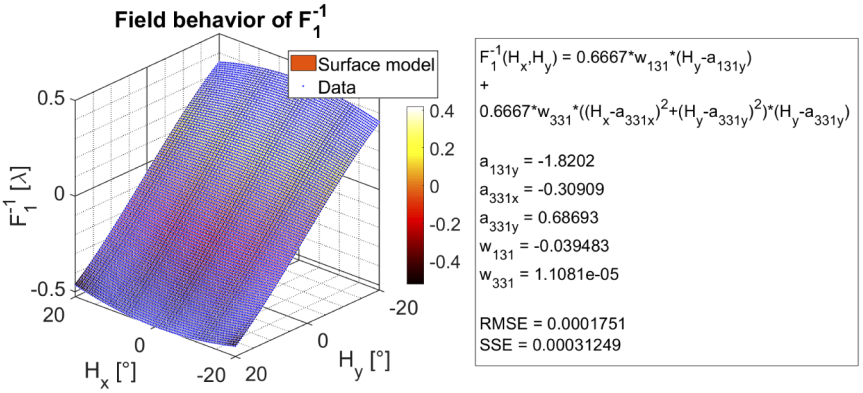

Fig. 6. Surface fitting of the field dependence of the third Zernike coefficient ($m = -1, n = 1$).

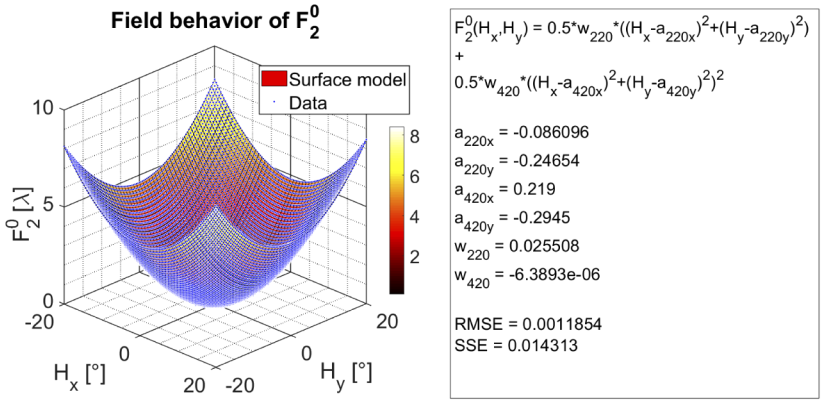

Fig. 7. Surface fitting of the field dependence of the fourth Zernike coefficient ($m = 0, n = 2$).

Regarding the surface fitting results in Figs. 8 and 9 for the field behavior of Zernike terms related to astigmatism, we can observe that the center of symmetry related to the field dependence of primary astigmatism is approximately the same in the two figures, being $\begin{pmatrix} a_{222,x} \\ a_{222,y} \end{pmatrix} = \begin{pmatrix} -0.11088° \\ -0.5631° \end{pmatrix}$ for Fig. 8 and $\begin{pmatrix} a_{222,x} \\ a_{222,y} \end{pmatrix} = \begin{pmatrix} -0.12509° \\ -0.57205° \end{pmatrix}$ for Fig. 9. The calculation of the center of symmetry of binodal astigmatism with Eq. (3) gives the following result $\begin{pmatrix} a_{222,x} \\ a_{222,y} \end{pmatrix} = \begin{pmatrix} 0.0135° \\ -0.4347° \end{pmatrix}$. The values of the aberration coefficients used for this calculation are relative to the tangential image surface. In practice, $W_{220T,j} = W_{220S,j} + W_{222,j}$ where the values of $W_{220S,j}$ and $W_{222,j}$ are those reported in Table 2 (with $j = \mathrm{L1}, \mathrm{L2}$) and $W_{220T,j}$ are the field curvature aberration coefficients referenced to the tangential image surface. We believe that this mismatch with the ray tracing data is due to the important role played by secondary aberrations. In both examples, for larger FOV the contribution of secondary astigmatism (characterized by its own center of symmetry not co-located with the center of symmetry of primary astigmatism) becomes more relevant. This can be observed in Fig. 9 where at the edge of the FOV ($H_x = 20°, H_y = 20°$) the field behavior of the sixth Zernike polynomial tends to be slightly curved.

OSA CONTINUUM

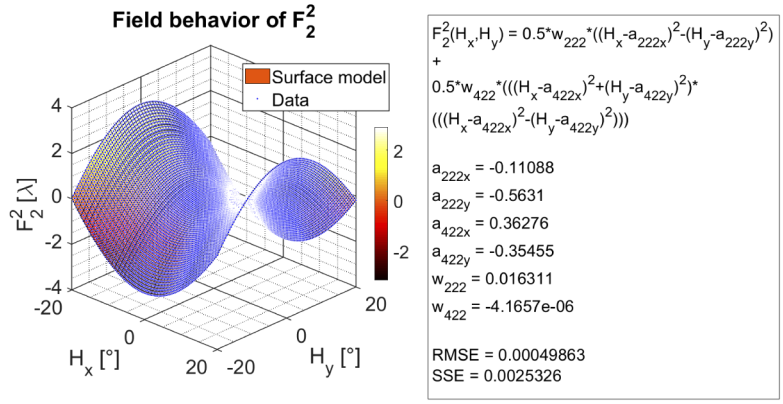

Fig. 8. Surface fitting of the field dependence of the fifth Zernike coefficient ($m = 2, n = 2$).

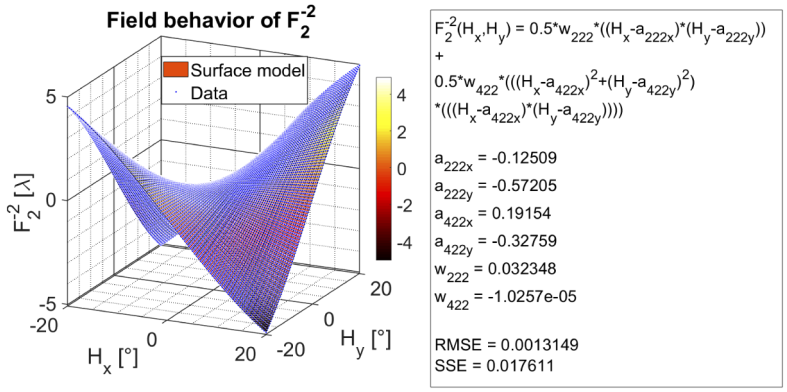

Fig. 9. Surface fitting of the field dependence of the sixth Zernike coefficient ($m = -2, n = 2$).

The surface fitting results shown in Figs. 10 and 11 for primary coma replicate what has been previously obtained for the second and third Zernike Fringe coefficients related to tilt along the H_x and H_y directions. The location of the center of symmetry in the FOV plane for primary

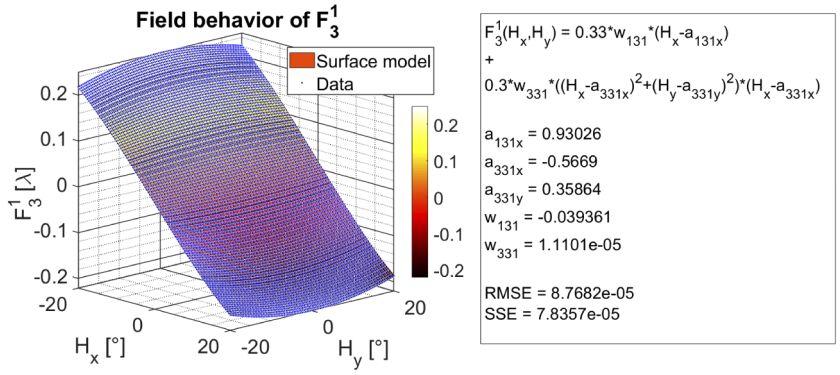

Fig. 10. Surface fitting of the field dependence of the seventh Zernike coefficient ($m = 1, n = 3$).

OSA CONTINUUM

coma is found to be $\begin{pmatrix} a_{131,x} \\ a_{131,y} \end{pmatrix} = \begin{pmatrix} 0.93026^\circ \\ -1.8207^\circ \end{pmatrix}$. For this type of aberration, as mentioned above, the location of its node in the FOV plane coincides with the center of symmetry of the field dependence of the inherent Zernike polynomials. In particular, the coordinate along the H_x direction is determined by the displacement related to the seventh Zernike term and the coordinate along the H_y direction is due to the eighth Zernike polynomial. Observing carefully Figs. 10 and 11, we can see that for larger values of the FOV the surfaces tend to be slightly "distorted". This behavior is due to the third order contribution (in the field coordinates) provided by field-cubed coma that has indeed the same field dependence of distortion so that the surfaces exhibit a barrel distortion-like deformation. Nonetheless, we point out that, even though such behavior is reminiscent of distortion, it cannot be ascribed to this type of aberration because, in line with the remarks above, distortion is not calculated with the ray tracing method presented here.

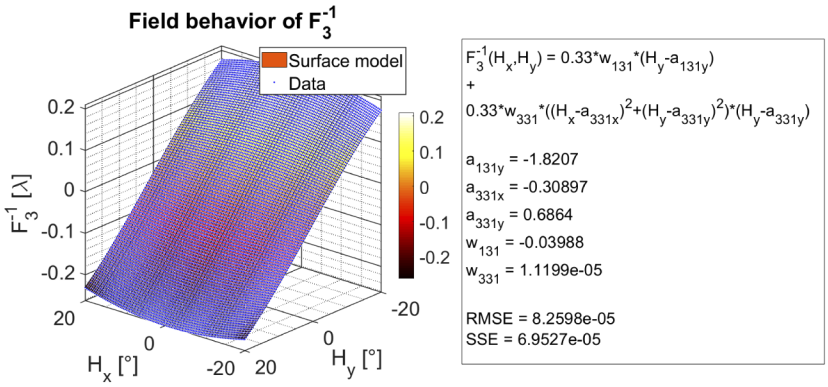

Fig. 11. Surface fitting of the field dependence of the eighth Zernike coefficient ($m = -1, n = 3$).

Finally, in Fig. 12 it is shown the surface fitting result obtained for the field behavior of the ninth Zernike Fringe coefficient dominated by the contribution of primary spherical aberration

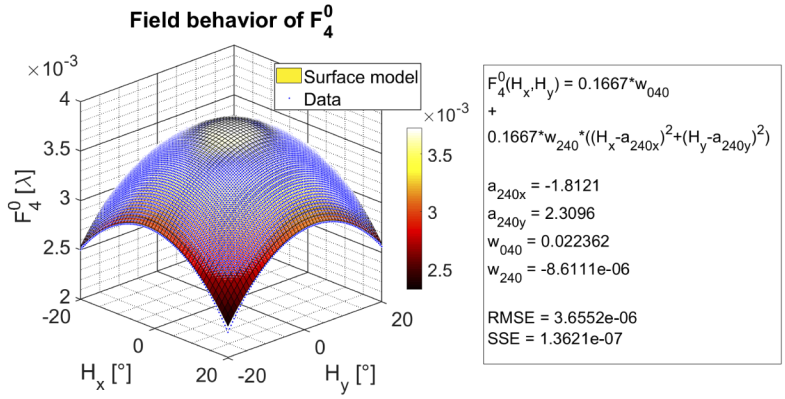

Fig. 12. Surface fitting of the field dependence of the ninth Zernike coefficient ($m = 0, n = 4$).

OSA CONTINUUM

and oblique spherical aberration. In this case, we can observe that the center of symmetry of the oblique spherical aberration is retrieved in the field point located in $\begin{pmatrix} a_{240,x} \\ a_{240,y} \end{pmatrix} = \begin{pmatrix} -1.8121^\circ \\ 2.3096^\circ \end{pmatrix}$.

5. Conclusions

In this paper, we have presented scalar analytical formulae describing the full field dependence of Zernike polynomials deriving from the field behavior of their inherent coefficients in asymmetric optical systems characterized by tilted and decentered circular symmetric surfaces. The starting point of such derivation is a modified version of the vectorial wavefront aberration function proposed in the Nodal Aberration theory. Such function is first transformed into its scalar counterpart, then it is projected onto the basis of Zernike polynomials in the Fringe indexing scheme in order to retrieve the full field behavior of individual Zernike coefficients. It is highlighted the presence of centers of symmetry for the field dependence of individual Zernike terms when they are described by the contribution of the only primary aberrations. Furthermore, it is emphasized that secondary aberrations change the symmetry of the field behavior of Zernike coefficients adding higher order overlay field surfaces with different centers of symmetry.

Funding

H2020 Marie Skłodowska-Curie Actions (675745).

Acknowledgments

This project has received funding from the European Union's Horizon 2020 research and innovation program under the Marie Sklodowska-Curie grant agreement No 675745.

Disclosures

The authors declare no conflicts of interest.

References

1. K. P. Thompson, "Description of the third-order optical aberrations of near-circular pupil optical systems without symmetry," J. Opt. Soc. Am. A **22**(7), 1389–1401 (2005).
2. K. P. Thompson, "Description of the third-order optical aberrations of near-circular pupil optical systems without symmetry: errata," J. Opt. Soc. Am. A **26**(3), 699 (2009).
3. H. H. Hopkins, *The Wave Theory of Aberrations* (Oxford on Clarendon Press, Oxford, UK, 1950).
4. R. W. Gray and J. P. Rolland, "Wavefront aberration function in terms of R. V. Shack's vector product and Zernike polynomial vectors," J. Opt. Soc. Am. A **32**(10), 1836–1847 (2015).
5. W. T. Welford, "Aberrations of Optical System," Adam Hilger Ltd (1986).
6. M. Rimmer, "Analysis of Perturbed Lens Systems," Appl. Opt. **9**(3), 533–537 (1970).
7. J. Sasián, "Theory of sixth-order wave aberrations," Appl. Opt. **49**(16), D69–D95 (2010).
8. K. P. Thompson, "Multinodal fifth-order optical aberrations of optical systems without rotational symmetry: spherical aberration," J. Opt. Soc. Am. A **26**(5), 1090–1100 (2009).
9. K. P. Thompson, "Multinodal fifth-order optical aberrations of optical systems without rotational symmetry: the comatic aberrations," J. Opt. Soc. Am. A **27**(6), 1490–1504 (2010).
10. K. P. Thompson, "Multinodal fifth-order optical aberrations of optical systems without rotational symmetry: the astigmatic aberrations," J. Opt. Soc. Am. A **28**(5), 821–836 (2011).
11. R. W. Gray, C. Dunn, K. P. Thompson, and J. P. Rolland, "An analytic expression for the field dependence of Zernike polynomials in rotationally symmetric optical systems," Opt. Express **20**(15), 16436–16449 (2012).
12. ZEMAX user guide, July 2018.
13. K. P. Thompson, T. Schmid, O. Cakmakci, and J. P. Rolland, "A real-ray based method for locating individual surface aberration field centers in imaging optical systems without rotational symmetry," J. Opt. Soc. Am. A **26**(6), 1503–1517 (2009).